NEOPLASIA
www.neoplasia.com

Volume 10 Number 12 December 2008 pp. 1459–1469 1459

Improved Magnetic Resonance Molecular Imaging of Tumor Angiogenesis by Avidin-Induced Clearance of Nonbound Bimodal Liposomes[1]

Geralda A.F. van Tilborg*, Willem J.M. Mulder†, Daisy W.J. van der Schaft*, Chris P.M. Reutelingsperger‡, Arjan W. Griffioen§, Gustav J. Strijkers* and Klaas Nicolay*

*Biomedical NMR, Department of Biomedical Engineering, Eindhoven University of Technology, Eindhoven, The Netherlands; †Translational and Molecular Imaging Institute, Mount Sinai School of Medicine, New York, NY, USA; ‡Department of Biochemistry, Cardiovascular Research Institute Maastricht, Maastricht University, Maastricht, The Netherlands; §Angiogenesis Laboratory, Department of Pathology, School for Oncology and Developmental Biology (GROW), Maastricht University, Maastricht, The Netherlands

Abstract

Angiogenic, that is, newly formed, blood vessels play an important role in tumor growth and metastasis and are a potential target for tumor treatment. In previous studies, the $\alpha_v\beta_3$ integrin, which is strongly expressed in angiogenic vessels, has been used as a target for Arg-Gly-Asp (RGD)–functionalized nanoparticulate contrast agents for magnetic resonance imaging–based visualization of angiogenesis. In the present study, the target-to-background ratio was increased by diminishing the nonspecific contrast enhancement originating from contrast material present in the blood pool. This was accomplished by the use of a so-called avidin chase, which allowed rapid clearance of nonbound paramagnetic RGD-biotin-liposomes from the blood circulation. C57BL/6 mice, bearing a B16F10 mouse melanoma, received RGD-functionalized or untargeted biotin-liposomes, which was followed by avidin infusion or no infusion. Precontrast, postcontrast, and postavidin T_1-weighted magnetic resonance images were acquired at 6.3 T. Postcontrast images showed similar percentages of contrast-enhanced pixels in the tumors of mice that received RGD-biotin-liposomes and biotin-liposomes. Post avidin infusion this percentage rapidly decreased to precontrast levels for biotin-liposomes, whereas a significant amount of contrast-enhanced pixels remained present for RGD-biotin-liposomes. These results showed that besides target-associated contrast agent, the circulating contrast agent contributed significantly to the contrast enhancement as well. *Ex vivo* fluorescence microscopy confirmed association of the RGD-biotin-liposomes to tumor endothelial cells both with and without avidin infusion, whereas biotin-liposomes were predominantly found within the vessel lumen. The clearance methodology presented in this study successfully enhanced the specificity of molecular magnetic resonance imaging and opens exciting possibilities for studying detection limits and targeting kinetics of site-directed contrast agents *in vivo*.

Neoplasia (2008) 10, 1459–1469

Abbreviations: ICP-AES, inductively coupled plasma atomic emission spectrometry; ICP-MS, inductively coupled plasma mass spectrometry; avidin-2-B4F, avidin-2-biotin-4-fluorescein

Address all correspondence to: Geralda A.F. van Tilborg, Eindhoven University of Technology, NLaag B2.03, Den Dolech 2, 5612 AZ Eindhoven, The Netherlands.
E-mail: g.a.f.v.tilborg@tue.nl

[1]This study was funded in part by the BSIK program entitled Molecular Imaging of Ischemic Heart Disease (project number BSIK03033) and by the EC – FP6-project DiMI, LSHB-CT-2005-512146. This study was performed in the framework of the European Cooperation in Scientific and Technical Research (COST) D38 Action Metal-Based Systems for Molecular Imaging Applications.
Received 25 July 2008; Revised 29 September 2008; Accepted 13 October 2008

DOI 10.1593/neo.08858

Introduction

Angiogenesis, the formation of new blood vessels from preexisting blood vessels, is an essential feature of tumor growth and metastasis [1]. Consequently, numerous angiogenesis inhibitors have been developed during the last years as novel therapeutic agents for the treatment of cancer [2]. Experimental and clinical studies have shown that antiangiogenic therapy can indeed cause tumor growth arrest or even tumor regression [3,4]. Within this research field, there is a great need for advanced diagnostic tools that allow for the detection of tumor angiogenesis *in vivo* because this would provide more and earlier insight in treatment efficacy at the molecular level and in a longitudinal fashion.

In the process of angiogenesis, activated endothelial cells upregulate the expression of the $\alpha_v\beta_3$ integrin, which binds to extracellular matrix components through their Arg-Gly-Asp (RGD) sequence. Experimental studies have shown that the $\alpha_v\beta_3$ integrin plays a pivotal role in angiogenesis because $\alpha_v\beta_3$ antagonists were able to inhibit tumor angiogenesis [5]. Furthermore, a low expression of the integrin is observed on resting endothelial cells, which makes the $\alpha_v\beta_3$ integrin an excellent molecular marker for tumor angiogenesis. Several studies have been performed, which used radiolabeled [6] or fluorescently labeled [7] cyclic RGD peptides for the *in vivo* detection of angiogenic blood vessels with either nuclear or optical imaging techniques. These techniques display a high detection sensitivity for the imaging probes, but they reveal little anatomic information. Therefore, RGD-conjugated gadolinium (Gd)–based [8–13] or iron oxide–based [14] magnetic contrast agents were proposed for the *in vivo* detection of tumor-associated $\alpha_v\beta_3$ expression using magnetic resonance imaging (MRI) because this technique provides excellent contrast of opaque soft tissue. Most of these Gd-based contrast agents were either based on liposomal [8,12,13] or on emulsion nanoparticles [10,11] that contain a large number of Gd^{3+} ions per particle to deal with the inherently low sensitivity of MRI. The average circulation half-life ($t_{1/2}$) of such RGD-conjugated particles, which is in the order of 2 to 8 hours [10,15,16], is significantly elevated compared with the intrinsic blood half-life of the RGD-peptide only (<10 minutes) [17]. A long blood half-life prolongs the time window during which the contrast agent can accumulate at the targeted site. However, long-circulating properties also allow prolonged time for extravasation, which, together with the blood pool contrast agent, gives rise to unspecific contrast enhancement in the T_1-weighted images because conventional T_1-weighted imaging does not allow discrimination between circulating, extravasated and target-associated contrast agent in the tumor. The contribution from the circulating contrast agents can be eliminated by acquiring the MR images when most of the contrast agent is cleared from the blood, as demonstrated in a study by Sipkins et al. [8]. In this study, MRI experiments were performed at 24 hours after injection of LM609 antibody-conjugated paramagnetic polymerized liposomes ($t_{1/2}$ ~ 8 hours) to enable target-specific imaging of tumor angiogenesis. Moreover, signal from flowing blood can be suppressed, which was shown to allow the visualization of contrast enhancement in atherosclerotic plaques in the abdominal aorta already at 1 hour after the injection of a long-circulating contrast agent ($t_{1/2}$ ~ 11 hours) [18]. However, flow suppression in tumors is not that straightforward owing to their complex and unstructured vasculature as well as the relatively low blood flow rates in tumor blood vessels compared to that in arteries [19,20]. Alternatively, in an experimental setting, a so-called avidin chase can be applied to remove circulating contrast agent from the blood. Avidin is a 66-kDa glycoprotein that displays a very short intrinsic blood half-life and can bind four biotin molecules with high affinity ($K_d < 10^{-15}$ M) [21]. Sinitsyn et al. [22] were the first to show that the biotin-avidin interaction can be used to rapidly clear long-circulating biotinylated antibodies from the blood. This clearance strategy has previously been used to increase the target-to-background ratio of radiolabeled biotinylated monoclonal antibodies (mAbs) [23] and liposomes [24] for nuclear imaging. The avidin chase has also been applied to biotinylated dendrimer-based [25] and albumin-based [26] MR contrast agents. Avidin-induced clearance of the latter agent allowed studying vascular permeability and extravascular drainage in tumors with MRI [26]. In previous studies, we showed that an avidin chase can also be used to rapidly clear bimodal, that is, fluorescently and gadolinium-labeled, biotin-liposomes from the blood pool [27]. In the present study, we applied a similar avidin chase, or no chase, to tumor-bearing mice that had been injected with either untargeted or RGD-functionalized bimodal biotinylated liposomes. T_1-weighted images were obtained precontrast, postcontrast, and postavidin infusion to assess the relative contributions of circulating, target-associated, and extravasated contrast agent to the signal enhancement. Fluorescence microscopy was performed to determine the spatial location of the contrast agent within the tumor *ex vivo*.

Materials and Methods

Materials

1,2-Distearoyl-*sn*-glycero-3-phosphocholine (DSPC), cholesterol, 1,2-distearoyl-*sn*-glycero-3-phosphoethanolamine-*N*-[methoxy(poly(ethylene glycol))-2000] (PEG2000-DSPE), 1,2-distearoyl-*sn*-glycero-3-phosphoethanolamine-*N*-[maleimide(poly(ethylene glycol))2000] (Mal-PEG2000-DSPE), 1,2-distearoyl-*sn*-glycero-3-phosphoethanolamine-*N*-[biotinyl(polyethylene glycol)2000] (biotin-PEG2000-DSPE) and 1,2-dioleoyl-*sn*-glycero-3-phosphoethanolamine-*N*-(lissamine rhodamine B sulfonyl) (rhodamine-PE) were obtained from Avanti Polar Lipids (Albaster, AL). Gd-DTPA-bis(stearylamide) (Gd-DTPA-BSA) was purchased from Gateway Chemical Technology (St. Louis, MO). Liposomes were sized with a Lipofast Extruder (Avestin, Ottawa, Ontario, Canada). Polycarbonate filters that were required for liposome extrusion were obtained from Costar (Cambridge, MA). HEPES, PBS, and paraformaldehyde were purchased from Sigma, Zwijndrecht, The Netherlands, and bovine serum albumin (BSA) was obtained from Fluka, Zwijndrecht, The Netherlands. All other chemicals were of analytic grade or of the best grade available.

Liposome Preparation

Paramagnetic liposomes were prepared by lipid film hydration of a lipid mixture that typically contained 100 μmol of total lipid. For biotinylated liposomes, Gd-DTPA-BSA, DSPC, cholesterol, Mal-PEG2000-DSPE, PEG2000-DSPE, and biotin-PEG2000-DSPE were used at a molar ratio of 0.75:1.1:1:0.075:0.045:0.03. Nonbiotinylated control liposomes contained Gd-DTPA-BSA, DSPC, cholesterol, Mal-PEG2000-DSPE, and PEG2000-DSPE at a molar ratio of 0.75:1.1:1:0.075:0.075. Lipid mixtures were dissolved in chloroform/methanol 2:1 (v/v), and 0.2 mol% rhodamine-PE was added for fluorescence microscopy. Subsequently, the solvent was removed by rotary evaporation, followed by additional drying under nitrogen. The dry lipid film was hydrated in 4 ml of HEPES-buffered saline (20 mM HEPES and 135 mM NaCl, pH 6.7) at 65°C. The resulting large

multilamellar vesicles were downsized to unilamellar liposomes by repetitive (>10×) extrusion at 65°C through a stack of two 200-nm filters.

Coupling of RGD

Acetyl-protected cyclic RGD peptide (c(RGDf(-*S*-acetylthioacetyl) K); Ansynth Service B.V., Roosendaal, The Netherlands) was activated in a deacetylation solution (0.05 M HEPES, 0.05 M hydroxylamine, 0.03 mM EDTA, pH 7.0) at a 1:10 v/v ratio for 1 hour. Subsequently, activated RGD peptide was added to the liposome suspensions at a final concentration of 6 μg/μmol total lipid to allow covalent conjugation of the RGD peptide to Mal-PEG2000-DSPE by sulfhydryl-maleimide coupling at 4°C overnight. Next, unbound RGD peptide was removed by ultracentrifugation (1 hour at 60,000 rpm), and liposomes were resuspended in HEPES buffered saline (20 mM HEPES and 135 mM NaCl, pH 7.4) to a final concentration of approximately 50 mM total lipid. The final lipid concentration was determined by a phosphate analysis according to Rouser et al. [28]. Dynamic light scattering was performed using Zetasizer Nano-S (Malvern Instruments, Malvern, UK) to determine the hydrodynamic size of the liposomes, as given by the intensity-weighted particle size distribution. Untargeted biotin-liposomes and RGD-biotin-liposomes were measured to have a mean diameter of 182 ± 8 nm and 190 ± 8 nm, respectively.

In Vitro Targeting

Target-specific association of RGD-liposomes to human umbilical vein–derived endothelial cells (HUVECs) was previously demonstrated both with confocal laser scanning microscopy and MRI [12]. In the present study, the target-specificity of RGD-biotin-liposomes for HUVEC was determined and compared to nonbiotinylated RGD-liposomes. Human umbilical vein–derived endothelial cells were cultured at 37°C in a humidified atmosphere and 5% CO_2 in medium RPMI-1640 (Life Technologies, Breda, The Netherlands), containing 20% human serum (University Hospital Maastricht, The Netherlands), 2 mM glutamine (Life Technologies), 100 U/ml penicillin, and 0.1 mg/ml streptomycin (ICN Biomedicals, Aurora, OH). For each cell sample, approximately 1×10^6 HUVECs were grown in gelatin-coated culture flasks. Cells were incubated with control-, RGD-, biotin- or RGD-biotin-liposomes for 3 hours at a final concentration of 1 mM total lipid in HUVEC culture medium at 37°C in a humidified atmosphere that contained 5% CO_2 in air. After incubation, cells were washed three times in warm HUVEC medium (37°C). Fluorescence microscopy images were obtained, and cells were washed once more in warm PBS (37°C). Next, HUVECs were harvested using a mild trypsinization procedure, washed in PBS, and resuspended in 4% paraformaldehyde (~100 μl). Loosely packed cell pellets were obtained by overnight settling in 250-μl polymerase chain reaction tubes. Subsequently, apparent T_1 values of the pellets were measured at 6.3 T (20°C) using a fast T_1 inversion recovery sequence with the following parameters: repetition time (TR) = 10 milliseconds, echo time (TE) = 3 milliseconds, flip angle (α) = 15°, number of excitations (NEX) = 2, matrix = 128 × 128, 32 segments, and 80 inversion times ranging from 67.5 to 4807.5 milliseconds. Full recovery of the magnetization between the different segments was allowed by using an overall repetition time of 20 seconds. T_1 values were calculated as described by Deichmann and Haase [29].

In Vivo Targeting

B16F10 melanoma cells were cultured in minimum essential medium supplemented with Hank's salts (Gibco, Invitrogen, Breda, The Netherlands), 10% fetal calf serum, antibiotics, minimum essential medium–vitamins, glutamine, nonessential amino acids, sodium pyruvate, and $NaHCO_3$. At the onset of the experiment, cells were harvested, and a total of 28 C57BL/6 mice (Charles River, Maastricht, The Netherlands) were inoculated subcutaneously with 1×10^5 B16F10 cells in 100 μl of PBS on the right hind leg. All experiments were approved by the animal ethical committee of Maastricht University.

Between 14 and 17 days after inoculation, the tumor size was considered appropriate for MRI. Mice with a mean weight of 27 ± 4 g were initially anesthetized with 3% isoflurane in medical air (0.4 L/min) that was supplied through a facemask. Anesthesia was maintained using 0.8% to 1.6% isoflurane in medical air (0.4 L/min). A catheter was placed in the tail vein, which allowed connecting to two different tubings for subsequent injection of the contrast agent and the avidin without prior mixture. Next, the avidin catheter was connected to a syringe pump (Pico Plus; Harvard Apparatus, Holliston, MA) that enabled infusion at a well-defined volume rate.

During the MR experiments, the mice were placed on a heating plate to regulate their body temperature, whereas the respiratory signal was monitored using a pressure sensor connected to an electrocardiogram trigger unit (Rapid Biomedical, Rimpar, Germany) to regulate the depth of the anesthesia. Each mouse received an intravenous bolus injection of RGD-biotin-liposomes (n = 14) or biotin-liposomes (n = 14), at a dose of 5 μmol of total lipid. For seven mice in each group, the infusion with avidin (0.2 mg/min; 2 mg total) was started approximately 1.5 hours after contrast agent administration (Figure 1), whereas the remaining mice (n = 7/group) were not infused at all.

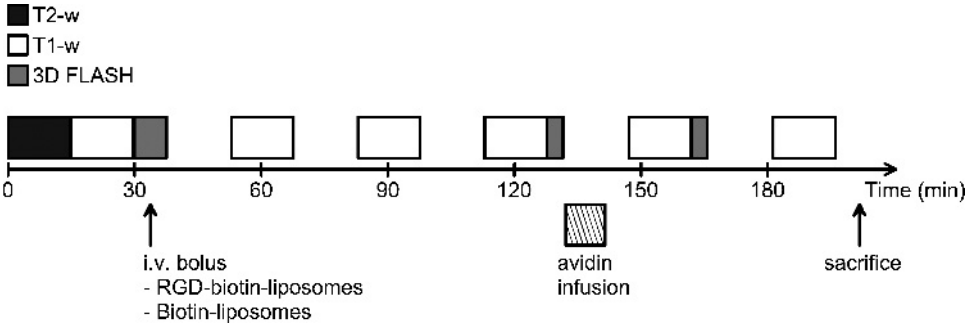

Figure 1. Time schedule of the *in vivo* MRI experiments.

Magnetic resonance imaging was performed at 6.3 T on a horizontal bore magnet (Oxford Instruments Superconductivity, Eynsham, Oxon, UK) interfaced to a Bruker imaging console (Bruker, Biospec, Ettlingen, Germany), using a 3-cm birdcage send and receive coil (Rapid Biomedical) for imaging. The time schedule of the complete MRI experiment is shown in Figure 1. Multislice T_2-weighted images were acquired to discriminate tumor tissue from the surrounding tissue using a fat-suppressed turbo spin echo sequence with TR = 4.2 seconds, TE = 25 milliseconds, turbo factor = 4, NEX = 8, matrix = 128 × 128, field of view (FOV) = 3 × 3 cm^2, and a slice thickness of 1 mm. T_1-weighted images were acquired to demonstrate contrast enhancement of tumor tissue using a fat-suppressed multislice spin echo sequence with the following parameters: TR = 800 milliseconds, TE = 8.8 milliseconds, NEX = 8, matrix = 128 × 128, and FOV = 3 × 3 cm^2. Slice positions of the T_1-weighted and T_2-weighted images were identical. Three-dimensional FLASH images were obtained to visualize the injection and clearance of the paramagnetic liposomes from the large vessels using the following imaging parameters: TR = 10 milliseconds, TE = 3 milliseconds, α = 30°, matrix = 128 × 128 × 64, and FOV = 3.2 × 3.2 × 4 cm^3. All precontrast imaging parameters and slice positions were exactly cloned for the corresponding postcontrast imaging sequences.

Directly after the MR experiments, blood samples were collected by orbital punction, mice were killed by cervical dislocation and organ tissues, namely, liver, spleen, kidney, lung, and muscle, were dissected and snap frozen in melting isopentane for fluorescence microscopy and inductively coupled plasma (ICP) analysis of gadolinium (Gd) content. Similarly, tumors were collected for fluorescence microscopy.

Magnetic Resonance Imaging Data Analysis

Small displacements in the animal position are difficult to avoid during avidin infusion, which contributes to errors when analyzing the contrast enhancement in the tumor tissue on a pixel-by-pixel basis. Therefore, we used a method where the signal intensity of each single pixel was compared to the average precontrast signal intensity within the tumor tissue for each individual mouse. First, two regions of interest (ROIs) were manually drawn in the T_2-weighted images, which included the tumor tissue and a small area within the noise, respectively. Next, the mean signal intensity within the tumor ROI was calculated for the corresponding slices in the precontrast T_1-weighted spin echo images ($SI_{tumorPre}$). The SD of the noise (SD_{noise}) in the T_1-weighted spin echo images was determined by the mean signal intensity within the noise ROI, divided by 1.25 [30]. Subsequently, a threshold was set for each imaging slice that was defined as $SI_{tumorPre} + 5 \cdot SD_{noise}$. Pixels within the tumor tissue were considered to be significantly enhanced when their signal intensity was higher than the threshold set for that specific imaging slice. Consequently, the precontrast image can also contain some pixels that are classified as enhanced according to this definition.

The method described above was used to determine the fraction of enhanced pixels within the total tumor for each individual mouse. Next, the fraction of enhanced pixels in the precontrast images was subtracted from the enhanced fractions in the corresponding postcontrast T_1-weighted spin echo images, resulting in the real fraction of contrast-enhanced pixels. From these values, the enhanced fractions were calculated and averaged for each group (n = 7/group) at every time point, resulting in a mean fraction ± SD. All data analyses were performed in Matlab, using a custom-built routine.

Statistical Analysis

A repeated-measures analysis of variance, with a Greenhouse-Geisser correction, was applied to detect time-dependent changes in contrast enhancement. *Post hoc* pairwise comparisons between the different time points, using a Bonferroni adjustment for multiple comparisons, were performed for each individual group of mice. Additional pairwise comparisons between RGD-biotin-liposomes and biotin-liposomes at each individual time point were performed using an unpaired Student's t test. For these tests, non–avidin-infused and avidin-infused mice were studied separately. Test statistics were considered to be significant for $P < .05$. All analyses were performed in SPSS 16.0.

Fluorescently Labeled Avidin

In the absence of an additional intervention, the avidin, as infused during the *in vivo* MRI experiments, could not be detected by fluorescence microscopy. Previous studies demonstrated that fluorescent avidin (avidin-2-B4F) has similar blood clearance kinetics as avidin [27]. Therefore, a total of three mice with a mean weight of 28 ± 2 g were infused with fluorescently labeled avidin (2 mg; 0.2 mg/min), starting approximately 1.5 hours after the intravenous administration of RGD-biotin-liposomes. Fluorescently labeled avidin (avidin-2-B4F) was freshly prepared before the experiment. For convenience, this was done by overnight incubation of avidin (Sigma) with biotin-4-fluorescein (Sigma) at a 1:2 molar ratio at 4°C, as described previously [27]. Approximately 1 hour after the onset of avidin infusion, mice were killed, following exactly the same time schedule as used for the *in vivo* MRI experiments. Tumors and organ tissues were excised and snap frozen in melting isopentane for fluorescence microscopy.

Fluorescence Immunohistochemistry

Tumor tissue sections of 5 μm were cut at −20°C. Sections were dried and stored at −80°C until the staining procedure was performed. Before each staining procedure, tissue sections were thawed, fixed for 5 minutes in cold acetone (−20°C), dried, and extensively washed in PBS. Subsequently, an immunohistochemical staining for endothelial cells was performed on all tumor tissue sections. First, sections were incubated with 20% FBS/1% BSA/PBS for 15 minutes. This solution was removed gently and immediately followed by incubation with the primary mAb rat antimouse CD31 (BD Pharmingen, Alphen aan de Rijn, The Netherlands), which was diluted to a 1:100 v/v ratio in 1% BSA in PBS. Tumor sections were incubated with the primary antibody for 2 hours at room temperature followed by extensive washing in PBS. Next, the sections were incubated for 1 hour with the secondary antibody goat antirat Ig-G fluorescein isothiocyanate (Zymed Laboratories, Invitrogen) at a 1:100 v/v ratio in 1% BSA and 5% mouse serum (animal facilities, Maastricht University) in PBS. Alternatively, tumor sections from mice that received avidin-2-B4F were incubated with goat antirat IgG Alexa Fluor 350 (Molecular Probes, Invitrogen) at a 1:200 v/v ratio under equivalent conditions. Each tissue section was again extensively washed in PBS. In between washing steps, sections that were incubated with the goat antirat Ig-G fluorescein isothiocyanate secondary antibody were counterstained for nuclei with 4′,6-diamidino-2-phenylindole (DAPI) (Molecular Probes, Invitrogen) at a final concentration of 0.1 μg/ml in PBS. After the staining procedure, tissue sections were covered with Mowiol mounting medium, and fluorescence microscopy images of the stained tissue sections were obtained using a fluorescence microscope (Zeiss, Sliedrecht, The Netherlands). Shutter times were adjusted for the

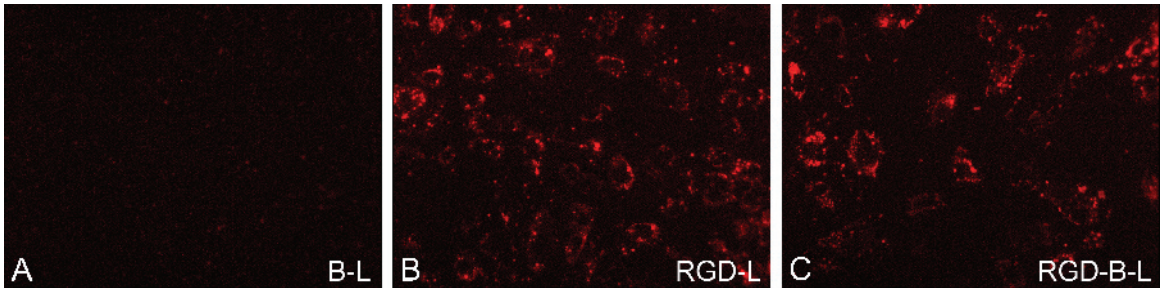

Figure 2. Fluorescence microscopy images of HUVEC that were incubated for 3 hours with (A) biotin-liposomes (B-L), (B) RGD-liposomes (RGD-L) or (C) RGD-biotin-liposomes (RGD-B-L), which contain rhodamine-PE (red). Original magnification, ×200.

non–avidin-infused and the avidin-infused mice to allow visualization of the liposomal rhodamine-lipid.

Biodistribution

The Gd content within the blood and the different organ tissues, namely, liver, spleen, kidney, lung, and muscle, was determined with ICP atomic emission spectrometry or mass spectrometry (ICP-AES/ICP-MS). In short, organ tissues and blood samples were weighed, placed in special tubes, and destructed in a mixture of perchloric and nitric acid at 170°C until a clear solution was obtained. The Gd contents within the solutions were determined using different dilutions of a Gd stock solution for calibration.

Results

In Vitro Targeting

Human umbilical vein–derived endothelial cells were incubated with nonbiotinylated or biotinylated paramagnetic liposomes, which were either untargeted or functionalized with RGD-peptides. Fluorescence microscopy images clearly demonstrated specific association of both the biotinylated and the nonbiotinylated RGD-functionalized liposomes to HUVEC, whereas marginal association was observed for both the untargeted nonbiotinylated (not shown) or untargeted biotin-liposomes (Figure 2).

Quantitative MR measurements on the fixed cell pellets were in good agreement with the fluorescence microscopy data, as relaxation rates R_1, that is, $1/T_1$, were only found to be largely increased in pellets of cells that were incubated with RGD-functionalized liposomes (both biotinylated and nonbiotinylated). In contrast, R_1 values were only slightly increased for cells that were incubated with the untargeted nonbiotinylated or biotin-liposomes in comparison to untreated control cells (Figure 3). Importantly, no significant effects of liposome biotinylation on target-specific or unspecific association of the liposomes to HUVEC were observed (Figure 3).

In Vivo Targeting

T_2-weighted images were used to discriminate the tumor tissue from surrounding muscle tissue, as the tumor tissue appeared hyperintense (Figure 4, *A* and *H*). In the precontrast T_1-weighted images, the tumors appeared essentially isointense with surrounding muscle, with exception of some hypointense necrotic areas and hyperintense regions in the tumor rim (Figure 4, *B* and *I*). After injection of the RGD-biotin-liposomes, the signal intensity in both tumor tissue and large blood vessels, for example, around the spine, was increased owing to the T_1 shortening effect of the paramagnetic liposomes (Figure 4, *C* and *J*). The spatial distribution of significantly contrast-enhanced pixels within the tumor was visualized by a color overlay on the original T_1-weighted image. As expected (Materials and Methods section), some pre–contrast-enhanced pixels were already present within the tumor because the signal intensity of these pixels was calculated to be above the threshold that was used (Figure 4, *E* and *L*). Without an avidin chase, most of the contrast enhancement within the tumor and the blood vessels persisted until at least 2.5 hours after contrast injection (Figure 4*D*). In these mice, most of the significantly contrast-enhanced pixels were found in the tumor rim (Figure 4*G*). Tumor tissue was also shown to be contrast-enhanced after the injection of untargeted biotin-liposomes (images not shown). No differences between the untargeted and RGD-functionalized biotin-liposomes were visually detected in the MR images.

The total fraction of contrast-enhanced pixels within the entire tumor was quantified to compare the contrast enhancement after injection with biotin-liposomes and RGD-biotin-liposomes. Approximately 30.8 ± 8.1% and 35.4 ± 6.7% of the tumor volume was found to be significantly enhanced at 30 minutes after the intravenous administration of the paramagnetic RGD-functionalized and untargeted biotin-liposomes, respectively (Figure 5*A*). Approximately 2.5 hours after injection of the RGD-biotin-liposomes, the enhanced fraction was reduced to 24.4 ± 9.9%, whereas 29.3 ± 5.7% of the

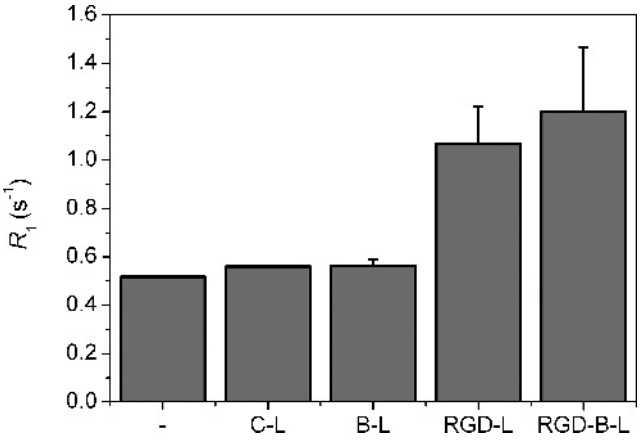

Figure 3. Longitudinal relaxation rates R_1 ($1/T_1$) of HUVEC cell pellets after incubation with control liposomes (C-L), biotin-liposomes (B-L), RGD-liposomes (RGD-L), or RGD-biotin-liposomes (RGD-B-L). Untreated control cells (−) were added for comparison. Bars represent mean R_1 values ± SD (n = 2/group).

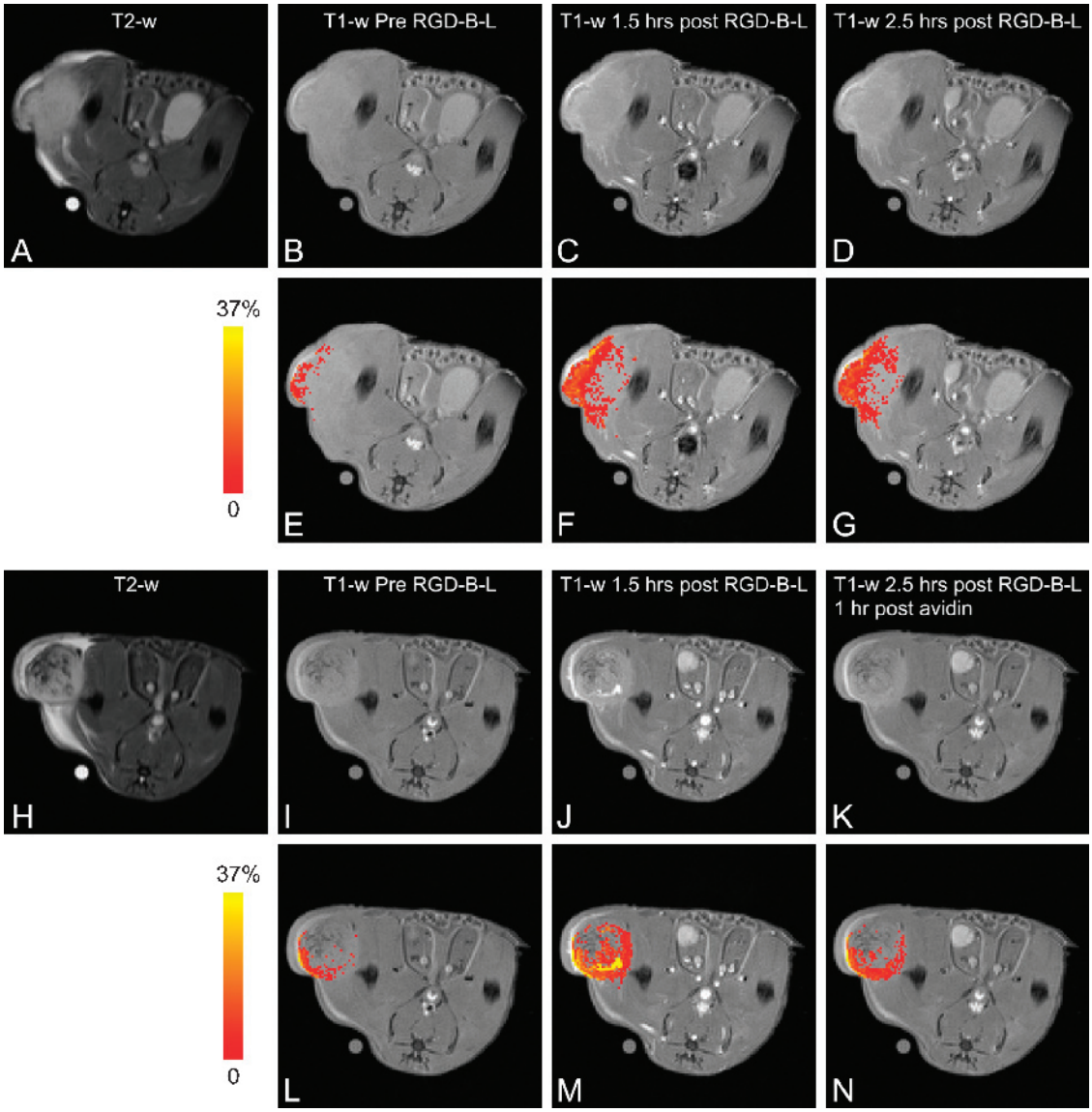

Figure 4. T_2-weighted (A, H) and T_1-weighted spin echo pre- and postcontrast MR images (B–G, I–N) of tumor-bearing mice that received an intravenous bolus of RGD-biotin-liposomes (RGD-B-L). The mouse in the upper panels (A–G) received no avidin. The mouse in the lower panels (H–N) was infused with avidin starting directly after the acquisition of the image shown in J. Pixels within the tumor tissue that were significantly enhanced are shown by a color overlay (E–G, L–N) on the corresponding T_1-weighted images in B–D and I–K, respectively. Color bar represents percentage of signal increase relative to the threshold value.

tumor tissue was shown to be enhanced for the untargeted biotin-liposomes. In these mice, no significant differences in the enhanced fractions were observed between the two contrast agents at any time point, which is in agreement with observations in a previous study [12].

In contrast to non–avidin-infused mice, the signal intensity in the large blood vessels of avidin-infused mice returned toward precontrast values within 1 hour after the onset of infusion, both in T_1-weighted spin echo images (Figure 4*K*) and T_1-weighted three-dimensional FLASH images (data not shown). These results indicate avidin-induced blood clearance of both biotin-liposomes and RGD-biotin-liposomes [27]. In mice that had previously received RGD-biotin-liposomes, the increased signal intensity within the tumor tissue was also visibly reduced within 1 hour after the onset of avidin infusion (Figure 4*K*). Most pixels that remained significantly enhanced were located in the tumor rim (Figure 4*N*).

For avidin-infused mice, the fractions of significantly enhanced pixels within the tumor were 26.7 ± 5.9% and 27.2 ± 8.2% at 30 minutes after injection of RGD-biotin-liposomes and untargeted biotin-liposomes, respectively (Figure 5*B*). For the RGD-biotin-liposomes, this fraction was significantly reduced to 10.3 ± 4.7% at 30 minutes and 6.2 ± 3.9% at 1 hour after the onset of avidin infusion. In mice that had been injected with biotin-liposomes, the percentage of enhanced pixels within the tumor was significantly decreased to 0.2 ± 2.4% and 1.4 ± 1.6% at the early and late time points after the onset of avidin infusion. Importantly, at those two time points, the contrast-enhanced fraction remaining after avidin infusion was significantly higher for the RGD-biotin-liposomes compared to the biotin-liposomes. No significant differences in tumor size were found between the different groups (Figure 5, *C* and *D*), which excludes that the above differences in MRI contrast changes were caused by differences in tumor size.

Fluorescence Immunohistochemistry

Fluorescence microscopy images demonstrated that the RGD-biotin-liposomes colocalized with endothelial cells within the tumor (Figure 6, *A* and *B*). Rhodamine fluorescence from these liposomes was also found within the vessel lumen. Biotin-liposomes were also detected within the lumen, whereas for this contrast agent, no endothelial cell association was observed (Figure 6, *C* and *D*). After the avidin chase, RGD-biotin-liposomes were found to remain colocalized with the endothelial cells (Figure 6, *E* and *F*). In this case, the liposomal fluorescence was more intense and clustered compared to mice that had received RGD-biotin-liposomes without avidin infusion. Intensely fluorescent liposomal clusters were occasionally also observed in the vessel lumen of avidin-infused mice that had been injected with biotin-liposomes (Figure 6, *G* and *H*).

Alternatively, three mice were infused with fluorescent avidin (avidin-2-B4F) after the injection of RGD-biotin-liposomes to visualize possible binding of avidin to target-associated contrast agents, and its role in the formation of the aggregates that were described above. Infusion with avidin-2-B4F clearly demonstrated that the intense fluorescent liposomal clusters of RGD-biotin-liposomes (Figure 7, *A* and *B*) colocalized both with avidin-2-B4F (Figure 7, *A* and *C*) and endothelial cells in the tumor (Figure 7, *A* and *D*).

Biodistribution

All mice were killed at approximately 170 minutes after the intravenous administration of the contrast agent. At this time point, significant quantities of both the RGD-biotin-liposomes and the biotin-liposomes were still present in the blood in case no avidin was infused (Figure 8*A*). The concentration of RGD-biotin-liposomes in the blood (60.9 ± 2.8 μg Gd/g tissue) was, however, slightly lower than that of the biotin-liposomes (91.7 ± 24.7 μg Gd/g tissue). In contrast, the amount of RGD-biotin-liposomes in the spleen (208.0 ± 7.1 μg Gd/g tissue) was higher compared to the biotin-liposomes (131.0 ± 7.1 μg Gd/g tissue), whereas Gd levels in liver, kidney, and lungs were comparable for the two liposomal preparations. In avidin-infused mice, the blood pool concentration of both contrast agents was decreased below 3.8 ± 0.7 μg Gd/g tissue, whereas the uptake in the spleen, liver, and lungs was found to be strongly increased (Figure 8*B*). In these avidin-infused mice, no differences in biodistribution were observed between the RGD-biotin-liposomes and the biotin-liposomes. No Gd uptake in skeletal muscle tissue was observed (data not shown).

Discussion

In the present study, we showed that an avidin chase can be used to rapidly clear nonbound RGD-functionalized or untargeted biotin-liposomes from the blood circulation, which facilitated early imaging and increased the specificity of target-specific MRI of tumor angiogenesis *in vivo*. Without avidin infusion, the RGD-functionalized and untargeted biotin-liposomes caused similar levels of contrast enhancement in T_1-weighted MR images of B16F10 mouse melanoma, which slowly decreased in time. In contrast, the percentage of contrast-enhanced pixels in avidin-infused mice was rapidly reduced after the onset of avidin infusion and resulted in a significantly higher contrast-enhanced fraction for the RGD-biotin-liposomes compared with the biotin-liposomes. The latter significant difference cannot be attributed

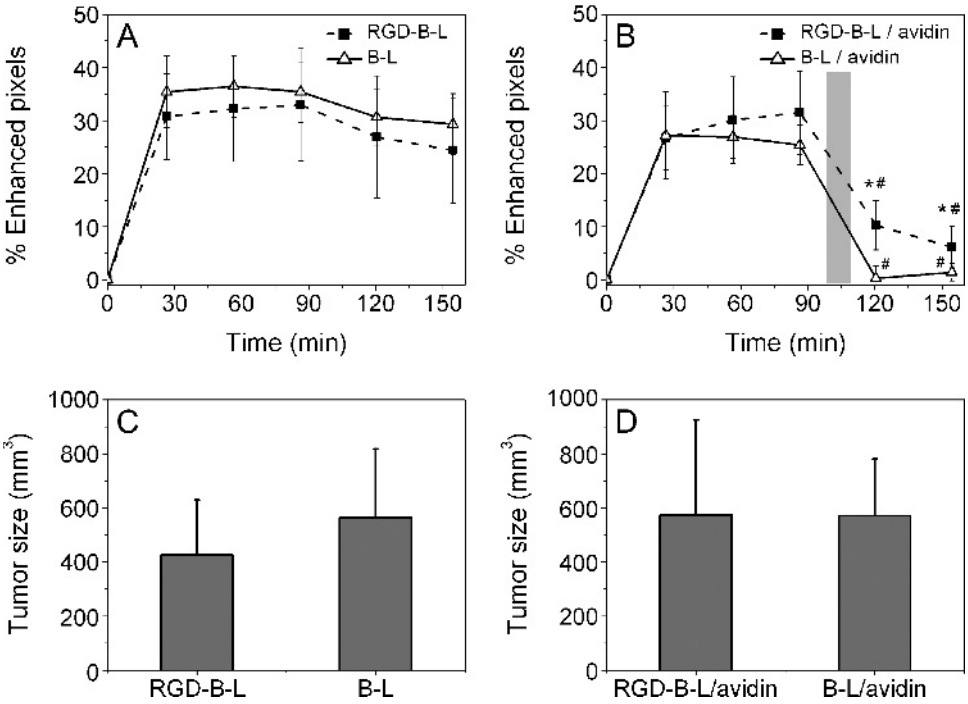

Figure 5. (A, B) Time dependence of the percentages of significantly contrast-enhanced pixels in T_1-weighted spin echo MR images of tumors after subtraction of the pre–contrast-enhanced fraction. RGD-biotin-liposomes (RGD-B-L) or biotin-liposomes (B-L) were injected at time 0. Subsequently, mice were left untreated (A) or avidin was infused between approximately 100 and 110 minutes after contrast agent injection as indicated by the gray bar (B). Data points represent the mean fraction of enhanced pixels ± SD (n = 7/group). *P < .05 between the two contrast agents at the given time point. #P < .05 relative to the first postcontrast time point. (C, D) Mean tumor sizes ± SD determined from the MR images for the different groups.

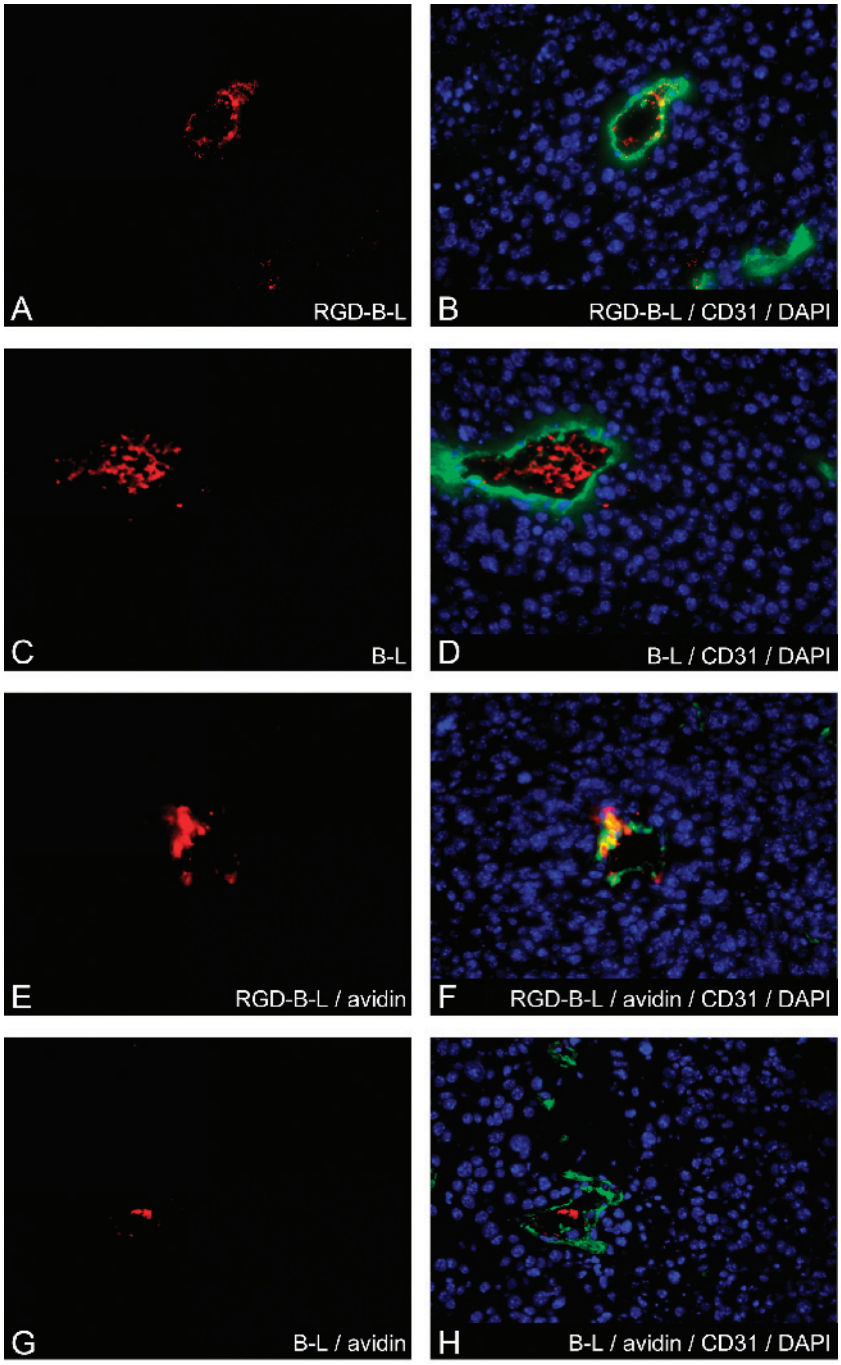

Figure 6. Fluorescence microscopy images of tumor sections from mice that received RGD-biotin-liposomes (A, B, E, F) or biotin-liposomes (C, D, G, H). Subsequently, mice were left untreated (A–D) or avidin was infused (E–H). Liposomal fluorescence from rhodamine-PE is shown in the left panel. Sections were costained for endothelial cells using an antimouse CD31 antibody (green), and for nuclei with DAPI (blue). Color overlays are shown in the right panel. Original magnification, ×400.

to differences in Gd levels in the blood because ICP measurements showed that the concentrations of Gd after the last imaging time point were were very low in both cases, that is, 0.015 ± 0.007 and 0.024 ± 0.004 mM for the RGD-biotin-liposomes and the biotin-liposomes, respectively. This is at least four times below the detection limits of the current MRI scan procedure. Therefore, a significant fraction of the contrast enhancement caused by RGD-biotin-liposomes in the tumors of non–avidin-infused mice is assumed to originate from target-associated contrast agent. The remaining contribution to the MRI contrast enhancement most likely originated from contrast agent circulating in the blood, which could potentially be used to determine the total tumor blood volume. The above interpretation of the data was confirmed by fluorescence microscopy, as before the avidin chase RGD-liposomes were found both in the vessel lumen and associated to the endothelial cells in the tumors. The relatively small percentage of pixels that remained enhanced within the tumors of avidin-infused mice that had first received biotin-liposomes strongly suggests that little extravasation of these liposomes had occurred in the relatively short time span of our study. This is supported by fluorescence microscopy images that showed only little extravascular fluorescence. Several studies presented

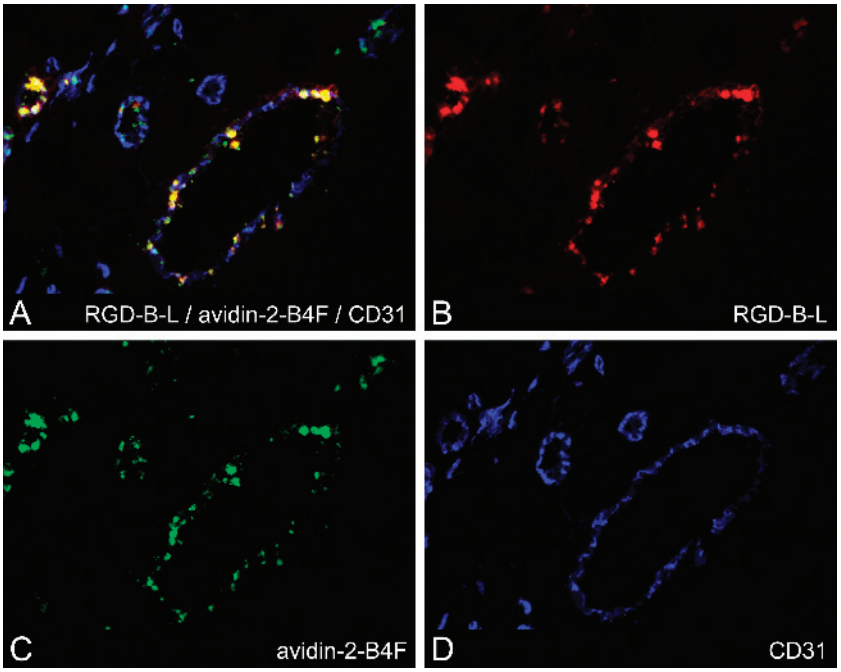

Figure 7. Fluorescence microscopy images of tumor sections from mice that had first been injected with RGD-biotin-liposomes, followed by an avidin-2-B4F chase. The overlay (A) is composed of signal from rhodamine-PE in the liposomes (B), fluorescent avidin (C), and endothelial cells, stained with an antimouse CD31 antibody (D). Original magnification, ×400.

in the literature showed that sterically stabilized liposomes indeed require considerable time to accumulate into tumors [31]. Interestingly, the avidin chase can also be exploited for dynamic studies on the extent of contrast agent extravasation *in vivo*. The actual rate and extent of liposome extravasation depends both on the tumor type and microenvironment, as well as the size, dose, formulation, and blood half-life of the liposomes [31,32]. In B16F10 melanoma tumor-bearing C57BL/6 mice, maximal accumulation of PEG-liposomes with a size of ~100 nm was observed around 16 hours after intravenous injection [33].

Calculated contrast-enhanced fractions of the tumor do not provide absolute numbers on the volume fraction of angiogenic blood vessels but only allows studying relative contributions of target-associated, extravasated, or circulating contrast agent. This is because the measured contrast-enhanced fractions are determined by multiple factors, including imaging sequence parameters, signal-to-noise, and data analysis criteria. Conventionally, contrast enhancement in MR images is quantified by comparing the postcontrast signal intensity of each single pixel to its precontrast signal intensity. However, pixel-by-pixel analysis could not be applied in the present study because a careful analysis of the time-course images revealed unacceptable displacements in the order of ≥2 pixels, when comparing images before and after the onset of avidin infusion. Consequently, we needed to resort to an alternative method of data analysis, in which the signal intensity was considered significantly contrast-enhanced above a threshold value that was determined by the average signal intensity in the tumor plus five times the standard deviation of the noise. In this manner, an unbiased threshold was set for each imaging slice. The disadvantage of this method is the occurrence of pre–contrast-enhanced pixels, which are excluded from the final post–contrast-enhanced fraction, even if they are further enhanced after contrast injection.

In the present study, the final contrast-enhanced fraction remaining after avidin infusion was 6.2 ± 3.9% in mice that received RGD-biotin-liposomes. We consider it likely that these values are relatively low owing to the large extent of necrosis in the fast-growing B16F10 tumor model. A slower-growing tumor model might have resulted in a larger fraction of target-associated contrast agent.

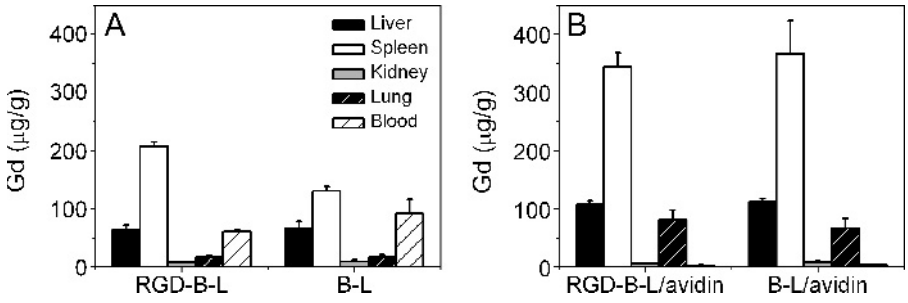

Figure 8. Biodistribution of RGD-biotin-liposomes (RGD-B-L) and biotin-liposomes (B-L) approximately 3 hours after intravenous liposomal administration, in mice that were subsequently left untreated (A) and in mice that were infused with avidin (B). Bars represent mean Gd content per tissue ± SD (n = 2/group).

Fluorescence microcopy images showed that avidin-2-B4F (Figure 7) colocalized with a substantial fraction of the endothelial cell–associated RGD-biotin-liposomes, which suggests limited internalization of this contrast agent *in vivo*. Consequently, the infusion of avidin may have dissociated a fraction of the membrane-bound RGD-biotin-liposomes from the endothelial cells owing to the high binding affinity of avidin to biotin. Moreover, avidin may also have bound to endothelial cell–associated RGD-biotin-liposomes without dissociating the contrast agent from these cells, which in turn could have recruited more RGD-biotin-liposomes from the blood pool to the targeted site through the biotin-avidin interaction. The latter effect indeed seemed to occur because avidin-induced liposomal aggregates were observed in the tumor, where they colocalized with the endothelial cells. Furthermore, binding of avidin-2-B4F to the cell-associated RGD-biotin-liposomes could have induced internalization of the RGD-biotin-liposome-avidin-2-B4F complex as previously observed for biotinylated mAbs [34] and dendrimers [35].

The onset of avidin infusion initiated an initial large drop in the percentage of contrast-enhanced pixels in the MR images in the RGD-biotin-liposome group, which was further decreased in a gradual manner. Possibly, this secondary decrease can be attributed to the gradual dissociation of some target-associated RGD-biotin-liposomes. In that case, some dissociation from the target may have also occurred at the early time point after avidin infusion. Moreover, the measured contrast enhancement could also suffer from partial quenching of the T_1 shortening caused by limited water exchange with the inside of the large target-associated liposomal aggregates that were formed by the avidin-infusion and/or caused by the internalization of these aggregates. Both partial dissociation and quenching of T_1 may lead to an underestimation of the contribution of the target-associated contrast agent to the observed contrast enhancement in T_1-weighted MR images.

Inductively coupled plasma analysis of the organ tissues showed a higher uptake of the RGD-biotin-liposomes by the spleen compared to the untargeted biotin-liposomes, whereas only little differences were observed between the targeted and the untargeted liposomes for the other organs. This is in agreement with previous studies reported in the literature, which predominantly showed receptor-dependent uptake of radiolabeled RGD by macrophages in the spleen and liver when compared to non–integrin-binding controls [17,36]. Radiolabeled long-circulating RGD-functionalized liposomes also showed significantly increased accumulation in the spleen at 24 hours after intravenous administration compared to control liposomes both in rats [16] and in mice [15], whereas no significant differences were observed in the liver. In those studies, the RGD-liposomes displayed a blood half-life in the order of 2 to 8 hours, which was increased by at least a factor 2 for control liposomes. Blood half-lives of the untargeted and the RGD-functionalized biotin-liposomes used in the present study were not determined. Alternatively, the blood levels of Gd were measured at 170 minutes after intravenous injection of the contrast agent. At this time point, the blood levels of RGD-biotin-liposomes were lower than those of biotin-liposomes. However, this difference was relatively small compared to the RGD-induced decrease in liposomal blood levels described in literature [15,16]. Differences in blood clearance kinetics between the biotin-liposomes used in the present study and the radiolabeled liposomes presented in literature could originate from several differences in experimental design, including liposome dose, liposome size, liposome composition, and the amount of RGD per liposome [37].

In previous studies, massive avidin-induced accumulation of biotin-liposomes was observed within the lungs at a spleen-to-lung ratio of ~1:2 [27]. In contrast, in the present study, the Gd content in the lungs on avidin infusion was relatively low, as the spleen-to-lung ratio was measured to be ~5.5:1. Most probably, this is caused by differences in the time point at which the avidin infusion was started because both the biotinylated liposomes and the avidin were administrated at the same dose and volume rate. In the previous study, the infusion of avidin was started at 30 minutes after injection of the contrast agent, whereas it was started after 1.5 hours in the present study. Consequently, the circulating levels of contrast agent were lower in the present study, probably leading to smaller liposomal clusters that were trapped by the lung capillaries to a smaller extent.

Over the last decades, liposomes were extensively applied as nanoparticulate drug carriers for cancer therapy to prevent drug degradation, inactivation, and adverse effects while increasing the amount of drug delivered to the tumor [38]. As discussed above, RGD-biotin-liposomes aggregate on the tumor endothelium of avidin-infused mice. This aggregation could be exploited as an amplification method to recruit large quantities of biotin-liposome–associated drugs to the tumor endothelium. For this purpose, a third injection with the drug-containing nanoparticle should be administered after the avidin chase. These so-called three-step labeling approaches have already been successfully applied to improve the target-to-background ratio in nuclear imaging, by radiolabeling biotinylated mAbs only at the targeted site after circulating mAbs were rapidly removed through an avidin chase [39]. Importantly, in the present experimental setup, only a relatively low dose of the nanoparticulate drug carrier would be required owing to the high binding affinity of biotin for avidin and the abundance of biotin at the targeted site.

In conclusion, the clearance strategy presented in this study can be used to investigate the relative contributions of target-associated, extravasated, and circulating nonbound contrast agent to the MRI contrast enhancement in the tumor tissue. This allows studying tumor vascularization and tumor angiogenesis in a single MRI experiment. Importantly, the presented strategy can be applied to remove the blood pool component in the contrast-enhanced MR images at various sites where flow suppression is not allowed or insufficient, which opens exciting possibilities for studying detection limits and targeting kinetics of target-specific MRI contrast agents *in vivo*.

Acknowledgments

The authors thank Petra Hautvast from the Angiogenesis Laboratory Maastricht for the assistance in the HUVEC experiments and Jeannette Smulders, Thea Haex, and Holger Gruell from Philips Research for the ICP measurements.

References

[1] Folkman J (1972). Anti-angiogenesis: new concept for therapy of solid tumors. *Ann Surg* **175**, 409–416.

[2] Folkman J (1997). Angiogenesis and angiogenesis inhibition: an overview. *EXS* **79**, 1–8.

[3] Griffioen AW and Molema G (2000). Angiogenesis: potentials for pharmacologic intervention in the treatment of cancer, cardiovascular diseases, and chronic inflammation. *Pharmacol Rev* **52**, 237–268.

[4] Kerbel R and Folkman J (2002). Clinical translation of angiogenesis inhibitors. *Nat Rev Cancer* **2**, 727–739.

[5] Brooks PC, Montgomery AM, Rosenfeld M, Reisfeld RA, Hu T, Klier G, and Cheresh DA (1994). Integrin alpha v beta 3 antagonists promote tumor regression by inducing apoptosis of angiogenic blood vessels. *Cell* **79**, 1157–1164.

[6] Liu S (2006). Radiolabeled multimeric cyclic RGD peptides as integrin alphavbeta3 targeted radiotracers for tumor imaging. *Mol Pharm* **3**, 472–487.

[7] Cai W, Shin DW, Chen K, Gheysens O, Cao Q, Wang SX, Gambhir SS, and Chen X (2006). Peptide-labeled near-infrared quantum dots for imaging tumor vasculature in living subjects. *Nano Lett* **6**, 669–676.

[8] Sipkins DA, Cheresh DA, Kazemi MR, Nevin LM, Bednarski MD, and Li KC (1998). Detection of tumor angiogenesis *in vivo* by alphaVbeta3–targeted magnetic resonance imaging. *Nat Med* **4**, 623–626.

[9] Ke T, Jeong EK, Wang X, Feng Y, Parker DL, and Lu ZR (2007). RGD targeted poly(L-glutamic acid)-cystamine-(Gd-DO3A) conjugate for detecting angiogenesis biomarker alpha(v) beta3 integrin with MRT, mapping. *Int J Nanomedicine* **2**, 191–199.

[10] Winter PM, Caruthers SD, Kassner A, Harris TD, Chinen LK, Allen JS, Lacy EK, Zhang H, Robertson JD, Wickline SA, et al. (2003). Molecular imaging of angiogenesis in nascent Vx-2 rabbit tumors using a novel alpha(nu)beta3–targeted nanoparticle and 1.5 tesla magnetic resonance imaging. *Cancer Res* **63**, 5838–5843.

[11] Schmieder AH, Winter PM, Caruthers SD, Harris TD, Williams TA, Allen JS, Lacy EK, Zhang H, Scott MJ, Hu G, et al. (2005). Molecular MR imaging of melanoma angiogenesis with alphanubeta3–targeted paramagnetic nanoparticles. *Magn Reson Med* **53**, 621–627.

[12] Mulder WJ, Strijkers GJ, Habets JW, Bleeker EJ, van der Schaft DW, Storm G, Koning GA, Griffioen AW, and Nicolay K (2005). MR molecular imaging and fluorescence microscopy for identification of activated tumor endothelium using a bimodal lipidic nanoparticle. *FASEB J* **19**, 2008–2010.

[13] Mulder WJ, van der Schaft DW, Hautvast PA, Strijkers GJ, Koning GA, Storm G, Mayo KH, Griffioen AW, and Nicolay K (2007). Early *in vivo* assessment of angiostatic therapy efficacy by molecular MRI. *FASEB J* **21**, 378–383.

[14] Zhang C, Jugold M, Woenne EC, Lammers T, Morgenstern B, Mueller MM, Zentgraf H, Bock M, Eisenhut M, Semmler W, et al. (2007). Specific targeting of tumor angiogenesis by RGD-conjugated ultrasmall superparamagnetic iron oxide particles using a clinical 1.5-T magnetic resonance scanner. *Cancer Res* **67**, 1555–1562.

[15] Schiffelers RM, Koning GA, ten Hagen TL, Fens MH, Schraa AJ, Janssen AP, Kok RJ, Molema G, and Storm G (2003). Anti-tumor efficacy of tumor vasculature–targeted liposomal doxorubicin. *J Control Release* **91**, 115–122.

[16] Koning GA, Schiffelers RM, Wauben MH, Kok RJ, Mastrobattista E, Molema G, ten Hagen TL, and Storm G (2006). Targeting of angiogenic endothelial cells at sites of inflammation by dexamethasone phosphate–containing RGD peptide liposomes inhibits experimental arthritis. *Arthritis Rheum* **54**, 1198–1208.

[17] Schraa AJ, Kok RJ, Moorlag HE, Bos EJ, Proost JH, Meijer DK, de Leij LF, and Molema G (2002). Targeting of RGD-modified proteins to tumor vasculature: a pharmacokinetic and cellular distribution study. *Int J Cancer* **102**, 469–475.

[18] Sirol M, Itskovich VV, Mani V, Aguinaldo JG, Fallon JT, Misselwitz B, Weinmann HJ, Fuster V, Toussaint JF, and Fayad ZA (2004). Lipid-rich atherosclerotic plaques detected by gadofluorine-enhanced *in vivo* magnetic resonance imaging. *Circulation* **109**, 2890–2896.

[19] McDonald DM and Choyke PL (2003). Imaging of angiogenesis: from microscope to clinic. *Nat Med* **9**, 713–725.

[20] McDonald DM and Baluk P (2005). Imaging of angiogenesis in inflamed airways and tumors: newly formed blood vessels are not alike and may be wildly abnormal: Parker B. Francis lecture. *Chest* **128**, 602S–608S.

[21] Schechter B, Silberman R, Arnon R, and Wilchek M (1990). Tissue distribution of avidin and streptavidin injected to mice. Effect of avidin carbohydrate, streptavidin truncation and exogenous biotin. *Eur J Biochem* **189**, 327–331.

[22] Sinitsyn VV, Mamontova AG, Checkneva YY, Shnyra AA, and Domogatsky SP (1989). Rapid blood clearance of biotinylated IgG after infusion of avidin. *J Nucl Med* **30**, 66–69.

[23] Kobayashi H, Sakahara H, Hosono M, Yao ZS, Toyama S, Endo K, and Konishi J (1994). Improved clearance of radiolabeled biotinylated monoclonal-antibody following the infusion of avidin as a chase without decreased accumulation in the target tumor. *J Nucl Med* **35**, 1677–1684.

[24] Laverman P, Zalipsky S, Oyen WJ, Dams ET, Storm G, Mullah N, Corstens FH, and Boerman OC (2000). Improved imaging of infections by avidin-induced clearance of ^{99m}Tc-biotin-PEG liposomes. *J Nucl Med* **41**, 912–918.

[25] Kobayashi H, Kawamoto S, Star RA, Waldmann TA, Brechbiel MW, and Choyke PL (2003). Activated clearance of a biotinylated macromolecular MRI contrast agent from the blood pool using an avidin chase. *Bioconjug Chem* **14**, 1044–1047.

[26] Dafni H, Gilead A, Nevo N, Eilam R, Harmelin A, and Neeman M (2003). Modulation of the pharmacokinetics of macromolecular contrast material by avidin chase: MRI, optical, and inductively coupled plasma mass spectrometry tracking of triply labeled albumin. *Magn Reson Med* **50**, 904–914.

[27] van Tilborg GA, Strijkers GJ, Pouget EM, Reutelingspeger CPM, Sommerdijk NAJM, Nicolay K, and Mulder WJM (2008). Kinetics of avidin-induced clearance of biotinylated bimodal liposomes for improved MR molecular imaging. *Magn Reson Med* **60**.

[28] Rouser G, Fkeischer S, and Yamamoto A (1970). Two dimensional then layer chromatographic separation of polar lipids and determination of phospholipids by phosphorus analysis of spots. *Lipids* **5**, 494–496.

[29] Deichmann R and Haase A (1992). Quantification of T1 values by Snapshot-FLASH NMR imaging. *J Magn Reson* **96**, 608–612.

[30] Haacke EM, Brown RW, Thompson MR, and Venkatesan R (1999). *Magnetic Resonance Imaging, Physical Principles and Sequence Design*. John Wiley & Sons, Inc., New York, NY.

[31] Drummond DC, Meyer O, Hong K, Kirpotin DB, and Papahadjopoulos D (1999). Optimizing liposomes for delivery of chemotherapeutic agents to solid tumors. *Pharmacol Rev* **51**, 691–743.

[32] Hobbs SK, Monsky WL, Yuan F, Roberts WG, Griffith L, Torchilin VP, and Jain RK (1998). Regulation of transport pathways in tumor vessels: role of tumor type and microenvironment. *Proc Natl Acad Sci USA* **95**, 4607–4612.

[33] Han HD, Lee A, Hwang T, Song CK, Seong H, Hyun J, and Shin BC (2007). Enhanced circulation time and antitumor activity of doxorubicin by comblike polymer-incorporated liposomes. *J Control Release* **120**, 161–168.

[34] Casalini P, Luison E, Menard S, Colnaghi MI, Paganelli G, and Canevari S (1997). Tumor pretargeting: role of avidin/streptavidin on monoclonal antibody internalization. *J Nucl Med* **38**, 1378–1381.

[35] Kobayashi H, Kawamoto S, Saga T, Sato N, Ishimori T, Konishi J, Ono K, Togashi K, and Brechbiel MW (2001). Avidin-dendrimer-(1B4M-Gd)(254): a tumor-targeting therapeutic agent for gadolinium neutron capture therapy of intraperitoneal disseminated tumor which can be monitored by MRI. *Bioconjug Chem* **12**, 587–593.

[36] Janssen ML, Oyen WJ, Dijkgraaf I, Massuger LF, Frielink C, Edwards DS, Rajopadhye M, Boonstra H, Corstens FH, and Boerman OC (2002). Tumor targeting with radiolabeled alpha(v)beta(3) integrin binding peptides in a nude mouse model. *Cancer Res* **62**, 6146–6151.

[37] Holig P, Bach M, Volkel T, Nahde T, Hoffmann S, Muller R, and Kontermann RE (2004). Novel RGD lipopeptides for the targeting of liposomes to integrin-expressing endothelial and melanoma cells. *Protein Eng Des Sel* **17**, 433–441.

[38] Torchilin VP (2007). Targeted pharmaceutical nanocarriers for cancer therapy and imaging. *AAPS J* **9**, E128–E147.

[39] Magnani P, Paganelli G, Modorati G, Zito F, Songini C, Sudati F, Koch P, Maecke HR, Brancato R, Siccardi AG, et al. (1996). Quantitative comparison of direct antibody labeling and tumor pretargeting in uveal melanoma. *J Nucl Med* **37**, 967–971.